A spatially distributed model for the long-term suspended sediment discharge and delivery ratio of drainage basins

Jon D. Pelletier[1]

Received 21 June 2011; revised 29 March 2012; accepted 2 April 2012; published 23 May 2012.

[1] Understanding and quantifying the long-term suspended sediment discharge of drainage basins is a key goal of geomorphology, with important implications for the study of water quality, agricultural sustainability, and the evolution of landscapes and sedimentary basins over geologic timescales. Previous studies have highlighted the importance of relief/slope, precipitation, temperature, vegetation, and soil texture in controlling suspended sediment discharge in natural/undisturbed landscapes. However, globally applicable models currently used to predict suspended sediment discharges are limited because they are based on basin-averaged versions of these properties and do not incorporate all of the controlling variables into a single model. In this paper, I propose a spatially distributed, globally applicable model for the long-term suspended sediment discharge of drainage basins that includes all of the principal controls on suspended sediment discharge previously documented in the geomorphic literature. The model explicitly distinguishes the detachment of sediment on hillslopes and in low-order valleys from the transport of sediment in higher-order alluvial channels. The model uses slope, soil texture, mean monthly rainfall, and mean monthly leaf area index as controlling parameters for the detachment component. The transport component is modeled using a Rouse number–dependent transport criterion that explicitly includes the effects of slope and soil texture. The model is capable of reproducing the long-term sediment yield of 128 global rivers with a Pearson correlation coefficient (R value) of 0.79 using just two free parameters. The model also predicts sediment delivery ratios consistent with those measured in natural drainage basins.

Citation: Pelletier, J. D. (2012), A spatially distributed model for the long-term suspended sediment discharge and delivery ratio of drainage basins, *J. Geophys. Res.*, *117*, F02028, doi:10.1029/2011JF002129.

1. Introduction

[2] Estimates of the long-term sediment discharge from drainage basins are important because they provide a measure of basin-averaged erosion rates. In particular, sediment discharges quantify the pace of landscape evolution [e.g., *Schumm*, 1963; *Young*, 1969] and they provide a baseline for assessing the impacts of modern agricultural practices and other land use changes on soil erosion and sediment discharge [e.g., *Hooke*, 2000; *Syvitski et al.*, 2005; *Syvitski and Milliman*, 2007; *Wilkinson and McElroy*, 2007]. Long-term in this context refers to time scales of decades to centuries, i.e., sufficiently long that estimated sediment discharges include the cumulative effects of many flood events but not so long that the estimates average over the effects of different climatic conditions. Estimates of sediment discharge are also important because sediment discharge is a principal boundary condition for terrestrial and marine depozones such as deltas and alluvial fans [e.g., *Paola*, 2000]. In order to understand how depositional basins have evolved over geologic timescales and to predict how they will evolve in the future, a better understanding of the controls on sediment discharge from drainage basins is needed. Quantifying sediment discharge from drainage basins remains a challenge in part because of the multiscale nature of the problem. Most sediment is sourced from hillslopes and low-order fluvial valleys, but predicting the sediment discharge to the ocean requires understanding how the sediment sourced from hillslopes and low-order valleys is stored in larger valleys, i.e., valleys with lengths up to $\sim$1000 km. In many drainage basins, a majority of the sediment eroded from upland hillslopes is deposited in lowland fluvial valleys [*Trimble*, 1977; *Phillips*, 1991; *Walling*, 1983]. Understanding the fate of that stored sediment, i.e., where it is stored and how and when it is remobilized, is important for predicting how fluvial systems will respond to future changes in climate and land use.

[3] Sediment discharge can be divided into a suspended-load component, i.e., sediment that moves in the water

[1]Department of Geosciences, University of Arizona, Tucson, Arizona, USA.

Corresponding author: J. D. Pelletier, Department of Geosciences, University of Arizona, 1040 E. Fourth St., Tucson, AZ 85721-0077, USA. (jdpellet@email.arizona.edu)

0148-0227/12/2011JF002129

column while only occasionally touching the bed, and a bed load component, i.e., sediment that moves close to the bed by repeated instances of rolling, sliding, and saltation. In most large river basins, i.e., those with drainage areas larger than $\sim$100 km^2, where both bed load and suspended load have been measured over a period of at least several years, suspended load is typically 80% or more of the total load [*Turowski et al.*, 2010]. In this paper, I focus on quantifying the controls on suspended load only because suspended load is the vast majority of the total load in most large rivers, and because it is arguably the most difficult component of the load to model. Suspended sediment discharge is hard to model because it depends on complex factors at many points throughout a drainage basin. Bed load, in contrast, depends primarily on local hydraulic factors in the vicinity of the point of measurement because tractive stresses must be maintained to transport bed load.

[4] Previous studies have emphasized the important roles played by topographic steepness (quantified as mean basin elevation, basin relief, or basin slope) [*Ahnert*, 1970; *Jansen and Painter*, 1974; *Hay et al.*, 1988; *Pinet and Souriau*, 1988; *Hovius*, 1998; *Milliman and Syvitski*, 1992; *Summerfield and Hulton*, 1994; *Ludwig and Probst*, 1998; *Mulder and Syvitski*, 1996; *Syvitski et al.*, 2003], precipitation or runoff (including seasonal variability) [*Langbein and Schumm*, 1958; *Fournier*, 1960; *Wilson*, 1973; *Summerfield and Hulton*, 1994; *Ludwig and Probst*, 1998; *Hovius*, 1998; *Syvitski et al.*, 2003; *Restrepo et al.*, 2006], temperature [*Jansen and Painter*, 1974; *Hovius*, 1998; *Syvitski et al.*, 2003], and vegetation cover/land use [*Douglas*, 1967; *Dunne*, 1979; *Ohmori*, 1983; *Milliman et al.*, 1987] on suspended sediment yields at regional to global scales. Sediment yield is defined as the sediment discharge (in metric tons per year, for example) divided by basin area. Normalizing by basin area in this way is useful because larger rivers, all else being equal, carry more sediment simply because of their greater size. Normalizing by basin area corrects for this effect and provides a measure of sediment discharge more closely related to erosion rate.

[5] Previous studies that have focused on the role of slope in controlling suspended sediment yields have documented an approximately linear correlation between sediment yield and relief for areas of low to moderate relief [e.g., *Ahnert*, 1970; *Pinet and Souriau*, 1988; *Ludwig and Probst*, 1998]. Low to moderate in this context refers to cases where topographic steepness is sufficiently low (i.e., less than or equal to approximately 20°) that mass movements do not occur in a significant portion of the drainage basin. The relationship between suspended sediment discharge and slope becomes significantly nonlinear in areas of steeper topography. The nonlinear relationship between suspended sediment yield and slope has been emphasized, in particular, by recent studies that have incorporated data from small, steep drainage basins [e.g., *Mulder and Syvitski*, 1996; *Montgomery and Brandon*, 2002; *Syvitski et al.*, 2003] in addition to the continental-scale drainage basins considered by classic studies such as *Jansen and Painter* [1974]. The nonlinear relationship between sediment yield and slope/relief can be quantified using a two-parameter model that includes a finite slope/relief at which nonlinear transport processes become significant [e.g., *Montgomery and Brandon*, 2002] or by using a one-parameter exponential [*Hovius*, 1998] or power law model (the latter with an exponent greater than one) [*Mulder and Syvitski*, 1996; *Syvitski et al.*, 2003]. In areas of similar relief, sediment yield increases approximately linearly with rainfall/runoff [*Jansen and Painter*, 1974; *Hovius*, 1998; *Ludwig and Probst*, 1998; *Restrepo et al.*, 2006] when differences in vegetation cover are taken into account.

[6] Suspended sediment yields have also been found to be very sensitive to vegetation cover and land use. *Dunne* [1979] found that sediment yield increased by up to two orders of magnitude as vegetation cover decreases from mostly forested to mostly agricultural to grazed conditions despite the similar slopes and climatic conditions of his study area in Kenya. It is unclear from *Dunne* [1979] whether the primary role of land use changes in controlling sediment yields is due to the decrease in vegetation cover or the disturbance of the soil by repeated instances of tilling and/or animal movement. *Ohmori* [1983] and *Vanacker et al.* [2007], however, have documented the sensitivity of sediment yields to vegetation cover in natural areas that have not undergone significant disturbance/land use changes. As such, vegetation cover is clearly an important control on suspended sediment yields whether or not it is accompanied by mechanical disturbance.

[7] Regression models have also documented that suspended sediment yields increase with increasing temperature [*Jansen and Painter*, 1974; *Hovius*, 1998; *Syvitski et al.*, 2003]. Temperature can control sediment discharge in at least four ways. First, higher mean temperatures can result in less precipitation falling as snow. Since snow does not disturb the soil to the same extent as rain splash, more soil disturbance will tend to occur in areas that experience more rainfall for the same precipitation, i.e., drainage basins in warmer climates. Second, drainage basins in warmer climates generally have less vegetation cover for otherwise similar conditions, due to the fact that evaporation rates are generally higher in warmer climates, all else being equal. Third, areas with higher temperatures generally have more finely textured soils due to the fact that chemical weathering rates increase with increasing temperature. Fourth, areas with higher temperatures have less erosion resistant frozen soil. Regression models that document the influence of temperature do not address the question of how temperature controls sediment yields, making it difficult to choose among competing regression models that quantify the role of temperature in different ways. In order to distinguish between the ways that temperature can influence sediment yields, it is necessary to explicitly quantify the direct controls exerted by rainfall (as distinct from precipitation), vegetation, and soil texture rather than use temperature as a proxy for some or all of these variables.

[8] In addition to these documented controls on sediment yields and sediment delivery ratios, soil texture has been anecdotally noted as an important control on suspended sediment yields. For example, the high suspended sediment yield of the Huang He (China) has been attributed, in part, to the fact that it drains large areas of highly erodible loess [e.g., *Ludwig and Probst*, 1998]. A soil composed of mostly silt will clearly be more erodible than a soil composed of mostly sand and gravel. Empirical models of soil erosion at the hillslope scale (e.g., USLE [*Wischmeier and Smith*, 1978]) incorporate a soil texture control, so available data clearly show that soil texture plays a role in controlling sediment discharge. At regional and global scales, however, few studies have quantified the effect

of soil texture on sediment yields. This may, in part, be due to a lack of high-quality, high-resolution data for soil texture globally. New global data sets, however, e.g., the Harmonized World Soils Map (available from the Harmonized World Soil Database, version 1.1, 2009, available at http://www.iiasa.ac.at/Research/LUC/External-World-soil-database/HTML), have greatly improved the quality of available data for soil texture in recent years. Several previous studies have correlated sediment yields to lithology as an alternative to soil texture [e.g., *Jansen and Painter*, 1974; *Beusen et al.*, 2005]. However, it is likely that the role of lithology (and structural properties such joint density that influence rates of soil production from bedrock) on sediment discharges is indirect because most sediment in alluvial rivers is sourced from soil on hillslopes rather than directly from bedrock via plucking, abrasion, or cavitation. Lithology likely influences sediment yields only insofar as it affects the availability of soil (e.g., some rock types are more weatherable and produce soil more rapidly than other types) and the texture of that soil. For this reason, I use soil texture rather than lithology in this study as the principal variable controlling substrate erodibility.

[9] An approximate inverse power law relationship exists between the sediment delivery ratio (defined as the ratio of the sediment yield at the basin outlet to the collective discharge of sediment from all of the hillslopes of the drainage basin) and basin area. Sediment delivery ratios provide a measure of sediment storage within the valleys of a drainage basin. Sediment delivery ratios are commonly found to decrease as an inverse power law function of drainage area with an exponent of approximately –0.1 such that small basins have sediment delivery ratios of between 0.3 and 1 (with higher values in steep basins and lower values in more gently sloping basins) and continental-scale drainage basins have sediment delivery ratios of ∼0.1 [e.g., *Roehl*, 1962; *Meade*, 1982; *Walling*, 1983]. This inverse power law relationship is generally interpreted to be the result of increased sediment storage due to size selective transport in the lowland floodplains of large drainage basins compared to smaller drainage basins. Although an inverse power law relationship is common, drainage area is certainly not the only control on sediment delivery ratios. Basin relief also controls sediment delivery ratios because steep drainage basins tend to have a lower potential for sediment storage relative to gently sloping basins of the same area. *De Vente et al.* [2007] noted that deviations from an inverse power law can occur in cases where lithology, land cover, climate and topography vary significantly with spatial scale.

[10] Many existing regression models that predict sediment discharge globally use basin-averaged properties to predict sediment yields. Clearly the suspended sediment discharged from a basin is not simply a function of the average steepness of that basin. Instead, it must be a function of the entire hypsometry. The Mississippi River basin, for example, has a complex morphology with much of the sediment storage potential controlled by the morphology of the lower Mississippi Valley. The basin relief ratio reduces the morphology of the Mississippi River basin to the ratio of just two numbers: the elevation of the highest point in the basin and the basin length. Similarly, the mean temperature of the Mississippi River basin or any other large drainage basin is of questionable value for quantifying the role of temperature on sediment yield in any particular portion of that basin. A large proportion of the sediment supplied by many drainage basins is sourced from only a small proportion of the basin where vegetation cover is lower than average, slopes are steeper than average, and conditions otherwise favor high sediment yields. As such, it is essential that models for suspended sediment yield be spatially distributed, i.e., that the resolve spatial variations in controlling variables to the greatest extent possible. In this paper I propose a model that computes sediment discharge/yield at every point on Earth using 5 arc min resolution input data instead of using basin-averaged properties. Sediment detached from hillslopes is routed through Earth's river systems to calculate the sediment discharge and sediment delivery ratio for every 5 arc min resolution pixel.

[11] *Osterkamp and Toy* [1997] highlighted the need for a more geomorphically based approach to modeling the sediment discharge from large drainage basins. While no model will ever include all of the processes controlling sediment discharges, models should be constructed to include the most important variables controlling the processes of detachment and transport within a spatially distributed model. A number of soil erosion models exist that can predict sediment yield from hillslopes and small drainage basins (e.g., USLE [*Wischmeier and Smith*, 1978], WEPP [*Laflen et al.*, 1991], etc.). However, no model exists that can account for the size selective transport and storage of sediment in drainage basins ranging in size from drainage areas of $\sim 10^2$ to 10^7 km^2. *Osterkamp and Toy* [1997] argued that we need models for predicting sediment yields that account for "(1) the complex set of geomorphic processes by which sediment becomes available for entrainment and transport, and (2) the storage of eroded sediment on the lower parts of hillslopes, on terraces, on the floodplain and other bottomland surfaces, and on channels." The aim of this paper is to partially fill the gap in geomorphically based models of suspended sediment yields of large drainage basins identified by *Osterkamp and Toy* [1997].

2. Model Description

2.1. Introduction to the Model Components

[12] The detachment and transport of sediment from hillslopes and low-order colluvium-filled valleys has been shown by many studies to be a nonlinear function of slope. The extensive empirical database used to calibrate the RUSLE model, for example, suggests that sediment yield from hillslopes increases approximately with slope to the 5/4 power. In order to capture this nonlinear relationship between sediment yield and slope, RUSLE uses one slope factor that is a linear function of slope for angles less than 9° and another, steeper linear function for angles greater than 9° [*McCool et al.*, 1987]. At slopes steeper than 22°, still another linear function is needed to reproduce the slope dependence of measured hillslope sediment yields. *Nearing* [1997], however, argued in favor of using a single continuous equation to capture this nonlinear slope dependence instead of using three different linear functions. *Nearing* [1997] proposed using

$$S_f = -1.5 + 17/[1 + \exp(2.3 - 6.1 \sin\theta)], \quad (1)$$

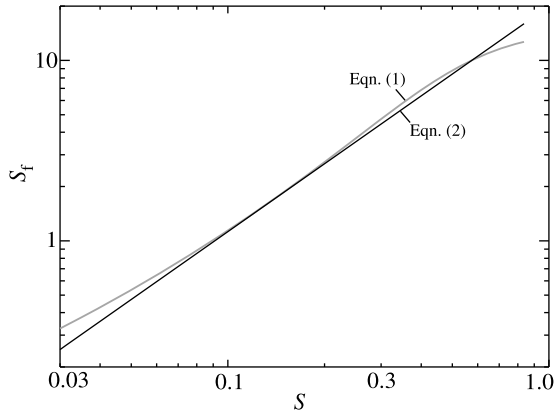

Figure 1. Plot of the slope factor, i.e., the factor increase in sediment yields due to increasing slope, for two alternative models, equation (1) (gray curve) and equation (2) (black line).

where S_f is the RUSLE slope factor and θ is the hillslope angle. Equation (1) has the disadvantage that the nonlinearity in slope decreases with increasing slope angle at relatively steep slope values (Figure 1). Sediment transport processes likely maintain or enhance their nonlinearity with increasing slope [e.g., *Roering et al.*, 1999]. Figure 1 plots (1) together with a power law function of slope with an exponent of 5/4, i.e.,

$$S_f = 20S^{5/4}, \tag{2}$$

where S is the tangent of the hillslope angle (dimensionless). As Figure 1 illustrates, the predictions of (1) and (2) are very similar, but (2) has the advantage of having a simpler form and maintaining a constant nonlinearity (i.e., the slope of the line in log-log space) with increasing slope. For these reasons I assume in the model of this paper that sediment detachment from hillslopes increases with the 5/4 power of slope.

[13] The model of this paper assumes that the rate of sediment detachment decreases as a constant factor for each unit increase in Leaf Area Index (LAI). LAI, defined as the ratio of the leaf area (oriented skyward) to the surface area of the ground on which the vegetation grows, is the property of vegetation most readily mapped over large areas (e.g., by satellites) that correlates strongly with the proportion of the surface protected from rain splash, gullying, and other sediment detachment processes. LAI values vary from 0 in arid regions to a maximum of approximately 8 in dense forests. Values greater than 1 indicate more than complete coverage, e.g., an LAI of 4 implies that on average, four leaf surfaces cover the ground along any vertical path.

[14] To motivate this proposed inverse relationship between sediment detachment rate and LAI, consider the fact that bare areas on hillslopes often produce the vast majority of sediment from a hillslope with bare and vegetated patches. *Prosser and Dietrich* [1995], for example, observed that in areas of complete vegetation cover, sediment transport was prevented for all but the most extreme overland flows. Figure 2 shows the relationship between the fraction of bare area and LAI in a simple stochastic model of vegetation cover on a hillslope. In the model, one pixel on a square grid is chosen at random and a unit of LAI is added to that pixel. Then, the process is repeated and the fraction of bare area is tracked as the average LAI of the hillslope increases with each model iteration. Due to the stochastic nature of the model, some pixels will acquire LAI values greater than 1 as more vegetation is added to the grid even as other pixels remain bare. Figure 2 shows that the fraction of bare area decreases as exp(–L) where L is LAI. If we assume that pixels with LAI values greater than 1 (complete coverage) produce relatively little sediment compared with bare areas, then suspended sediment yield should correlate strongly with the fraction of bare area. The results of Figure 2 suggest that an exponential relationship between suspended sediment yield and LAI is a reasonable first-order representation of the role of vegetation in reducing the detachment of soil particles from hillslopes and low-order channels.

[15] Once sediment is liberated from hillslopes and low-order valleys using the detachment component of the model, its transport is controlled by the ratio of the fluvial forces that drive transport (i.e., slope, flow depth) to the forces that resist transport (i.e., grain diameter, sediment density). In the model of this paper I use a proxy for the Rouse number, defined as the ratio of the grain settling velocity to the product of the von Karman constant and the shear velocity, as the criterion to identify which of the sediments delivered from hillslopes and low-order valleys will be transported in higher-order alluvial channels downstream as suspended load.

2.2. Numerical Model

[16] The numerical model of this paper computes the rate of sediment detachment in each pixel of the model using

$$D(x, y, d) = c_1 \rho_b f_d S^{5/4} \sum_{k=1..12} R_k e^{-L_k}, \tag{3}$$

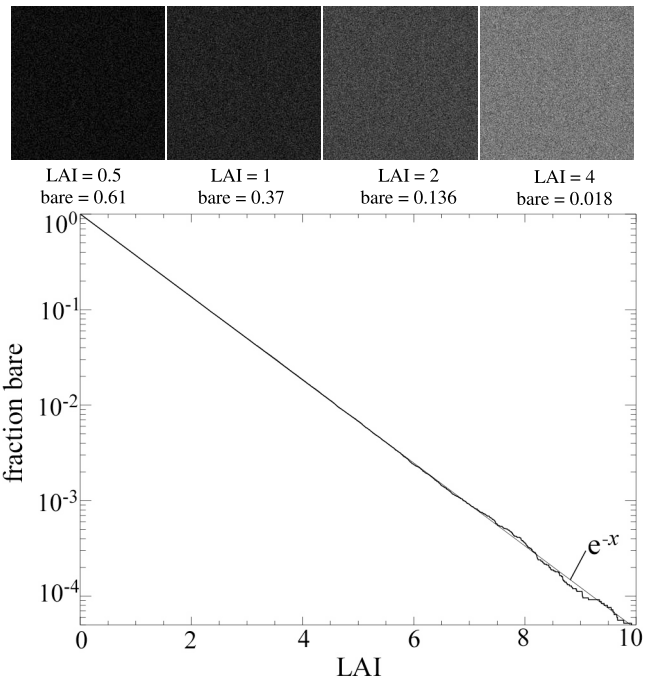

Figure 2. Plot of the fraction of bare area versus leaf area index (LAI) (both dimensionless) for the stochastic vegetation model described in the text. The data follow the form exp(–x).

where $D(x,y,d)$ is the detachment rate (kg m^{-2} yr^{-1}) computed at every location (x,y) and for every grain diameter d; c_1 is a free parameter (dimensionless) calibrated to measured global sediment discharge data; ρ_b is the bulk density of the soil (kg m^{-3}) (assumed to be 1500 kg m^{-3}); f_d is the fraction of the soil within each soil texture bin of grain diameter d (dimensionless); S is slope (dimensionless); R_k is the mean monthly rainfall (indexed by k, which varies from 1 (January) to 12 (December) (m yr^{-1})); and L_k is the mean monthly LAI (dimensionless). The free parameter c_1 quantifies the local erosion rate from the hillslopes and low-order valleys within each pixel of the model using values for slope, rainfall rate, and LAI. The value of f_d is computed by dividing the full range of grain diameters from clay to gravel into a set of discrete intervals or bins, each centered on a grain diameter d. Soil texture maps are then used to estimate the fraction of the soil within each bin. By computing rainfall and vegetation on a monthly basis, (3) captures the effect of seasonal covariation in rainfall and vegetation on soil erosion.

[17] The detachment rate computed by (3) is synonymous with the sediment yield from hillslopes or small drainage basins because sediment routing through the fluvial system in the model occurs at a scale larger than the size of one pixel, i.e., 5 arc min or a width of approximately 10 km at the equator (but smaller at higher latitudes). The model of this paper operates on a 5 arc min resolution grid. Hillslopes and channels are not explicitly resolved in the model due to the limited resolution of the input data. Instead, detachment takes place from every 5 arc min by 5 arc min pixel as a function of the slope (and other controlling variables) calculated between that pixel and its neighbor along the direction of steepest descent. Because the detachment rate is slope-dependent, the steeper "headwater" pixels will supply the majority of the sediment load, whereas the lower-gradient pixels associated with distal portions of the drainage system will supply very little, hence they function mostly to transport or store what is delivered from upstream. Slopes calculated at 5 arc min resolution will tend to underpredict the steepest slope values at the hillslope scale. However, since the model is calibrated to the observed sediment flux data, it is not necessary that the slopes calculated at the 5 arc min scale match slopes at the hillslopes scale precisely. Instead, it is only necessary that the slopes at the 5 arc min scale be highly correlated with slopes at the hillslope scale, since the model has a degree of freedom in the coefficient c_1 that can implicitly account for variations in systematic biases in slope values as a function of scale.

[18] In order to use (3) to determine the sediment discharge in large drainage basins, the model uses the detachment rate as input to a sediment routing model that uses the Rouse number as the criterion for determining whether or not sediment is transported in suspension to the next pixel downstream in the fluvial system. In this routing model, sediment supplied to the fluvial system from hillslopes within each pixel is added to the sediment that has been routed to that pixel from all upstream pixels. Sediment is routed in suspension from that pixel to the steepest downstream pixel if the Rouse number is less than 1.2 (the transition between suspended load and bed load). In every pixel of the model, the Rouse number for each grain size bin is calculated independently to determine whether or not the sediment of that particular size class is transported. In this way, relatively steep portions of the landscape will transport all but the coarsest fractions of sediment delivered to them, while lower-gradient areas will store a larger fraction of the total sediments delivered to them. Sediment is routed first from the pixel with the highest elevation on Earth (which, by definition, has no upstream tributaries). Routing then proceeds to each lower pixel in rank order of elevation. This ordering ensures that when the routing algorithm acts on a particular pixel, all of the sediment delivered to that pixel from all of the contributing pixels upstream has already been calculated.

[19] The grain sizes capable of being transported in suspension are determined by the Rouse number, $R_\#$, i.e.,

$$R_\# = \frac{w_s}{\kappa u_*}. \tag{4}$$

The shear velocity is defined as

$$u_* = \sqrt{ghS}, \tag{5}$$

where g is the acceleration due to gravity (m s^{-2}) and h is the instantaneous flow depth (m). Equation (5) uses the small-angle approximation $\sin\theta \approx S$, which is appropriate in this case since (5) is being applied to the transport of sediments in fluvial valleys ranging from drainage areas of $\sim 10^2$ to 10^7 km^2 with slopes in the range of 10^{-5} to 10^{-1}.

[20] As (4) and (5) show, the Rouse number is a function of instantaneous flow conditions. This poses a challenge for this particular application because what is needed is a Rouse number characteristic of long-term transport conditions. The simplest approach to this problem is to not include the effects of varying flow depth on the shear velocity but instead to assume that the shear velocity is a function of slope only. Channel slopes on Earth vary over approximately 4 orders of magnitude (from 10^{-5} to 10^{-1}) while flow depths during high-flow conditions vary over only approximately 1 order of magnitude, i.e., from approximately 1 m in small ($\sim 10^2$–10^3 km^2) drainage basins to approximately 10 m in large ($\sim 10^6$–10^7 km^2) drainage basins. Given the relatively small variation in h compared to S and the difficulty of identifying a unique value for h characteristic of transport conditions over time scales of decades to centuries, it is reasonable as a first approximation to assume that shear velocity is a function of slope only. The Rouse number in the model, therefore, is calculated as

$$R_\#(x,y,d) = c_2 \frac{w_s}{S^{1/2}}, \tag{6}$$

where w_s is computed using the formula of *Ferguson and Church* [2004] and c_2 is a free parameter with units of s m^{-1} determined by calibration to the database of sediment yield from 128 global rivers. In section 3 I consider the sensitivity of the model predictions to the different assumed power law relationships between Rouse number and channel slope. In the model, sediment is transported to the next pixel downstream if the local value of $R_\#$ computed by (6) is less than 1.2, otherwise it is stored or transported as bed load.

[21] Available soil texture data quantify the fraction of gravel, sand, silt, and clay in the soil. In order to apply (3) and (6), however, it is necessary to estimate the proportion

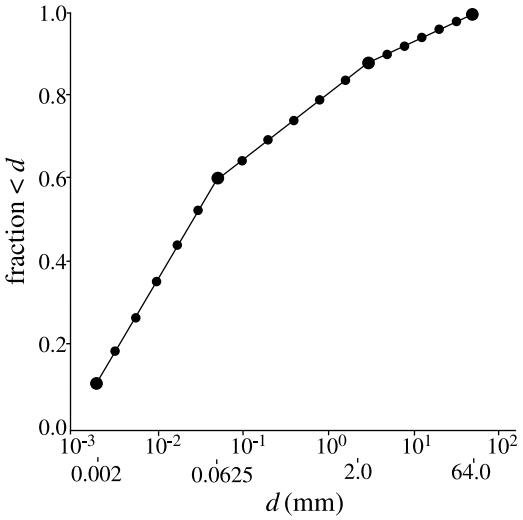

Figure 3. Schematic illustration of the interpolation procedure used to estimate the fraction of soil in each bin of grain diameter *d.* The figure plots the fraction of soil with a diameter less than *d* as a function of *d.* Input data provide the fractions of soil in the clay, silt, sand, and gravel fractions (shown as large circles). The model of this paper interpolates (in logarithmically spaced bins of *d*) between the known fractions at every pixel in the model grid (interpolated points shown as small circles).

of soil within relatively narrow discrete bins of grain diameter *d.* In this paper I assume that the fractions of soil within logarithmically spaced bins can be linearly interpolated as a function of *d* between the known fractions at $d = 0.002$ mm (upper end of the clay range), 0.0625 mm (upper end of silt), 2 mm (upper end of sand), and 64 mm (upper end of gravel). This approach is illustrated schematically in Figure 3. The example in Figure 3 shows a soil with 10% clay, 50% silt, 30% sand, and 10% gravel. In the model, the range of grain diameters from 0.002 mm to 64 mm is divided into 18 logarithmically spaced bins.

2.3. Input Data Layers and Database of Measured Sediment Discharges

[22] The model requires precisely corectified input data layers for topography, fractions of clay, silt, sand, and gravel, mean monthly rainfall, and mean monthly LAI. This is a total of 29 input data layers, each with 4320 columns and 1800 rows.

[23] I used the 5 arc min resolution Digital Elevation Model (DEM) of the WorldClim project [*Hijmans et al.*, 2005] as the input topography for the model. This DEM was derived from the Shuttle Radar Topography Mission (SRTM) topographic data set. Within the model this DEM is used to create 4 additional layers: slope (Figure 4), the area of each pixel (varies with latitude), flow direction, and drainage area.

[24] Data for river slopes are highly inaccurate if they are calculated as the difference between adjacent pixels within a relatively low resolution DEM. However, whether sediments of a given grain size are transported or not depends sensitively on channel slope via the Rouse number–dependent transport criterion utilized by the model. As such, it is necessary to combine two different approaches in order to construct a slope map of adequate quality for the purposes of the model of this paper. First, the slope was calculated as the difference between two adjacent pixels along the direction of steepest descent. In mountainous topography this approach provides an accurate estimate of slope within the limitations posed by the resolution of the input DEM. Second, the slope was calculated as the ratio of the elevation of each pixel to the along-channel distance from that pixel to the ocean. This second method of slope measurement provides a more accurate estimate of slope in low-gradient river systems compared to that of the first method. The slope map used as input to the model of this paper uses the maximum of the two slope values calculated using these two methods. In this way, the slopes of relatively steep mountainous areas are derived from the usual method of steepest descent while the slopes of relatively low gradient rivers are based on the average slope from that point to the ocean.

[25] The input data layers for mean monthly rainfall were created using a preprocessing step that uses input data for mean monthly precipitation and temperature from the WorldClim project [*Hijmans et al.*, 2005] (Figure 4). Mean monthly rainfall was computed from mean monthly precipitation and temperature by assuming that all of the precipitation that falls during any month with a mean temperature of less than 0°C falls as snow, otherwise it is assumed to be rain. Input data layers for mean monthly LAI were computed from gridded Normalized Difference Vegetation Index (NDVI) data sets from 1981 to 2006 using data collected by the Advanced Very High Resolution Radiometer (AVHRR) instrument and provided to the research community by the Global Land Cover Facility of the University of Maryland [*Tucker et al.*, 2004]. To convert NDVI values to LAI, I used the method of *Sellers et al.* [1996]. The resulting values of LAI ranged from near 0 (desert) to approximately 8 (dense rain forest) (Figure 4). Gridded data sets for the fractions of clay, silt, sand, and gravel were constructed from the Harmonized World Soil Database, version 1.1 (2009, available at http://www.iiasa.ac.at/Research/LUC/External-World-soil-database/HTML). I used the FWTools package (http://fwtools.maptools.org/) to perform the Geographic Information System (GIS) operations necessary to obtain a precisely corectified set of raster grids for each input layer.

[26] The database of this paper includes the best-available estimates of the natural/predam sediment discharge of 128 rivers (auxiliary material).[1] Natural/predam in this context refers to the fact that sediment discharge data collected prior to dam emplacement was used to the greatest extent possible and/or the discharges have been adjusted to account for the effects of flow regulation and sediment trapping of dams to the greatest extent possible. The database of this paper is similar to that of *Mulder and Syvitski* [1995, 1996], with two key differences. First, sediment yields for a small number of basins were corrected based on the revised natural/predam suspended sediment yields published by *Peucker-Ehrenbrink* [2009]. *Peucker-Ehrenbrink* [2009] explicitly distinguished natural/predam estimates of sediment yield from estimates that do not correct for the influence of dams and flow regulation, minimizing the uncertainty associated with whether a

[1]Auxiliary materials are available at ftp://ftp.agu.org/apend/jf/2011jf002129.

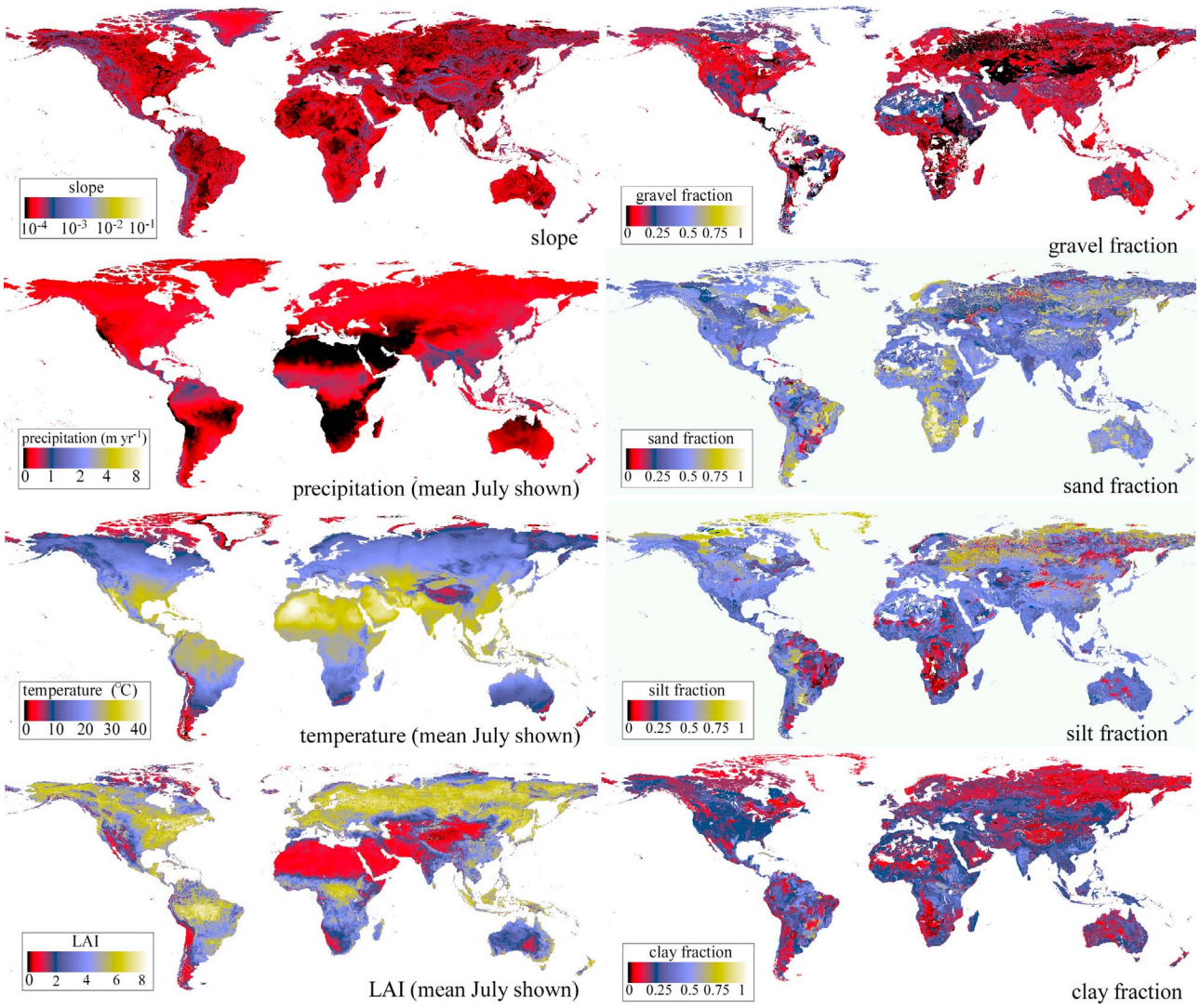

Figure 4. Color maps of the input data used in the model, including topography (used to determine slope), mean monthly precipitation, temperature, and leaf area index (LAI) (July only is shown) showing fractions of gravel, sand, silt, and clay.

given estimate is or is not appropriate for natural/predam conditions. Second, many of the smaller basins in the *Mulder and Syvitski* [1995, 1996] and *Peucker-Ehrenbrink* [2009] databases are not included here due to the difficulty of precisely locating those basins in the model grid. In order to calibrate and compare the model to the observed data, it was necessary to identify the exact pixel within the model grid that represents the location of the river just upstream from its delta. For large rivers this was a simple task. For some smaller rivers, however, i.e., those with drainage areas of $\sim 10^3$–10^4 km^2, this was a significant challenge because some of these basins comprise less than a few dozen pixels in the model grid.

3. Results

[27] Figure 5a plots the predicted versus modeled long-term sediment yields corresponding to the best fit values of the 2 free parameters of the model, $c_1 = 1.5 \times 10^{-7}$ and $c_2 = 300$ s m^{-1}. The best fit values for c_1 and c_2 were obtained using a brute force trial-and-error procedure that identified the pair of values with the lowest sum of the squared differences between the logarithms of the measured data and the model predictions (Figure 5b). Figure 5b presents a gray scale map of the error values for each value of c_1 and c_2 as c_1 was varied from 0.03 to 0.3, and c_2 was varied from 50 to 500 s m^{-1}. As Figure 5b shows, the error value is minimized for $c_1 = 0.15$ and $c_2 = 300$ s m^{-1}. Figure 5a illustrates that the model does a reasonably good job of reproducing the observed sediment yields ($R = 0.79$), especially given that the model contains just two free parameters. The model of this paper produces just one river (the Sous in Morocco) where the predicted load is more than 30 times higher or lower than the measured yield. To further test the model, I also plotted the difference between the predicted and observed values as a function of mean basin slope, discharge, temperature, and LAI (results not shown) and verified that those residuals did not show any

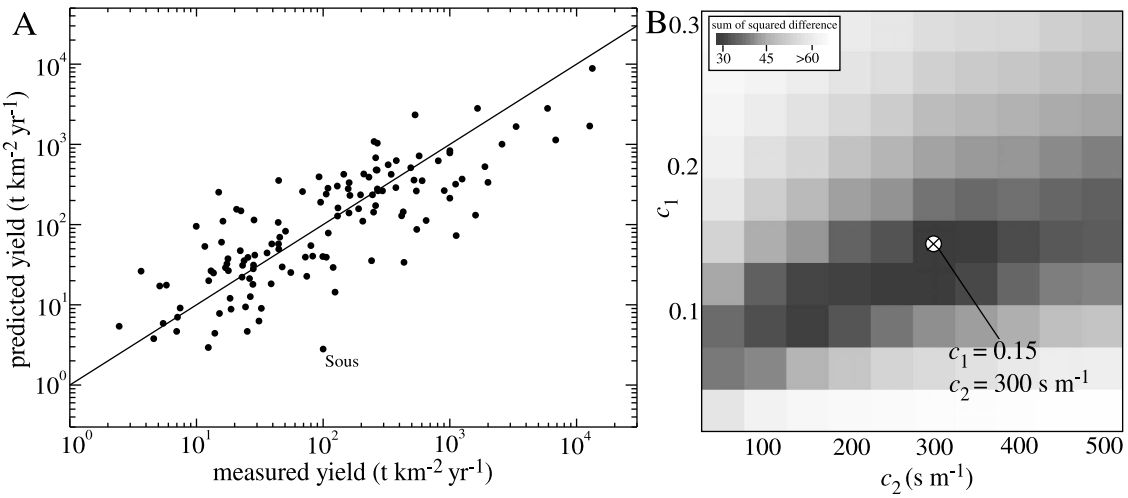

Figure 5. Results of the calibration of the model of this paper (i.e., equations (3) and (6) and the sediment routing algorithm). (a) Plot of the predicted versus observed suspended sediment yield, with a Pearson correlation coefficient (R value) of 0.79. (b) Gray scale map of the error values (computed as the sum of squared difference between the logarithm of each measured data point and the logarithm of each model prediction). The best fit (i.e., lowest error) results occur for $c_1 = 0.15$ and $c_2 = 300$ s m^{-1}.

trends. This additional test suggests that the model is optimally capturing the effects of each controlling variable.

[28] Figure 6 illustrates global maps of the sediment detachment rate (from (3)), sediment yield (from the full sediment routing model using (3) and (6)) and the sediment delivery ratio (the inverse of the sediment delivery ratio value is shown because otherwise low sediment delivery ratio values are hard to see in the map). The map of detachment rate (Figure 6a) is strongly correlated with the slope map of Figure 4, reflecting the important control played by slope in the detachment component of the model. Rainfall and vegetation play important roles also, but on a global basis the effect of slope is particularly apparent because of the large range of variability in slope compared to these other controlling variables. The natural/predam sediment yield also correlates strongly with slope (Figure 6b). Sediment delivery ratios are smaller in larger basins, more arid basins, and in lower-relief basins (Figure 6c).

[29] Figure 7 illustrates the results of the model for three example drainage basins: the Amazon (Figure 7a), the Ob (Figure 7b), and the Nile (Figure 7c). Figure 7a illustrates that the model predicts relatively high sediment yields in the Andes Mountains. Sediment yields decrease systematically with increasing drainage area in Figure 7a, reflecting the fact that yields decrease with distance from the Andes because some of the sediment delivered from the Andes is stored in lowland rivers and because drainage area (the denominator in sediment yield) increases downstream. Figure 7b shows the sediment yield map of the Ob River (Russia). Note that the color scale of Figure 7b had is adjusted relative to those of Figures 7a and 7c because the yields of the Ob basin are much smaller than those of the Amazon and Nile Rivers due to the gently sloping nature of the topography and the cold (snow-dominated) climate. The sediment yield map of the Nile drainage basin shows that most of the sediment delivered to the Nile is sourced from tributaries incised into the Ethiopian Plateau. The model does an excellent job at predicting the measured sediment discharges of the Amazon and Ob Rivers, but somewhat overpredicts the suspended sediment yield of the Nile River.

[30] Figure 8 illustrates several key scaling relationships exhibited by the model (shown as light gray circles in Figures 8a–8c) along with a comparison to measured data in Figures 8b and 8c (dark gray circles). Figure 8a plots the sediment delivery ratios predicted by the model against drainage area. The model results plotted in Figure 8 include results for 1% (randomly sampled) of all the land surface pixels in the model. I subsampled the data in this way to avoid having to plot millions of points and because this subsample shows the same trends as those observed when all of the model pixels are plotted. The model predicts that sediment delivery ratios decrease as a power law function of drainage area with an exponent of approximately –0.1 (shown as the straight line in this log-log plot). Black circles joined with lines represent logarithmically binned arithmetic means of the model predictions. This pattern of model predictions is broadly similar to that of data reported in the literature; i.e., sediment delivery ratios decrease as an inverse power law function of drainage area with an exponent of approximately 0.1, decreasing from values between 0.1 and 1 to values of approximately 0.1 for continental-scale (i.e., $\sim 10^6$–10^7 km^2) drainage basins [e.g., *Roehl*, 1962; *Meade*, 1982; *Walling*, 1983].

[31] Figure 8b plots sediment yield as a function of drainage area for the model (light gray circles) and the measured data (darker gray circles). The model predicts that sediment yield decreases relatively slowly with increasing drainage area; i.e., the model follows a power law trend similar to that for sediment delivery ratio in Figure 8a. By comparison, the measured data decrease much more rapidly with increasing drainage area. This difference may be due to a sampling bias in the measured data. The measured data include all or nearly all of the larger drainage basins on Earth regardless of their location or their relative yield. Many of the small drainage basins in the data set, however, were included precisely because they have large yields (e.g., the

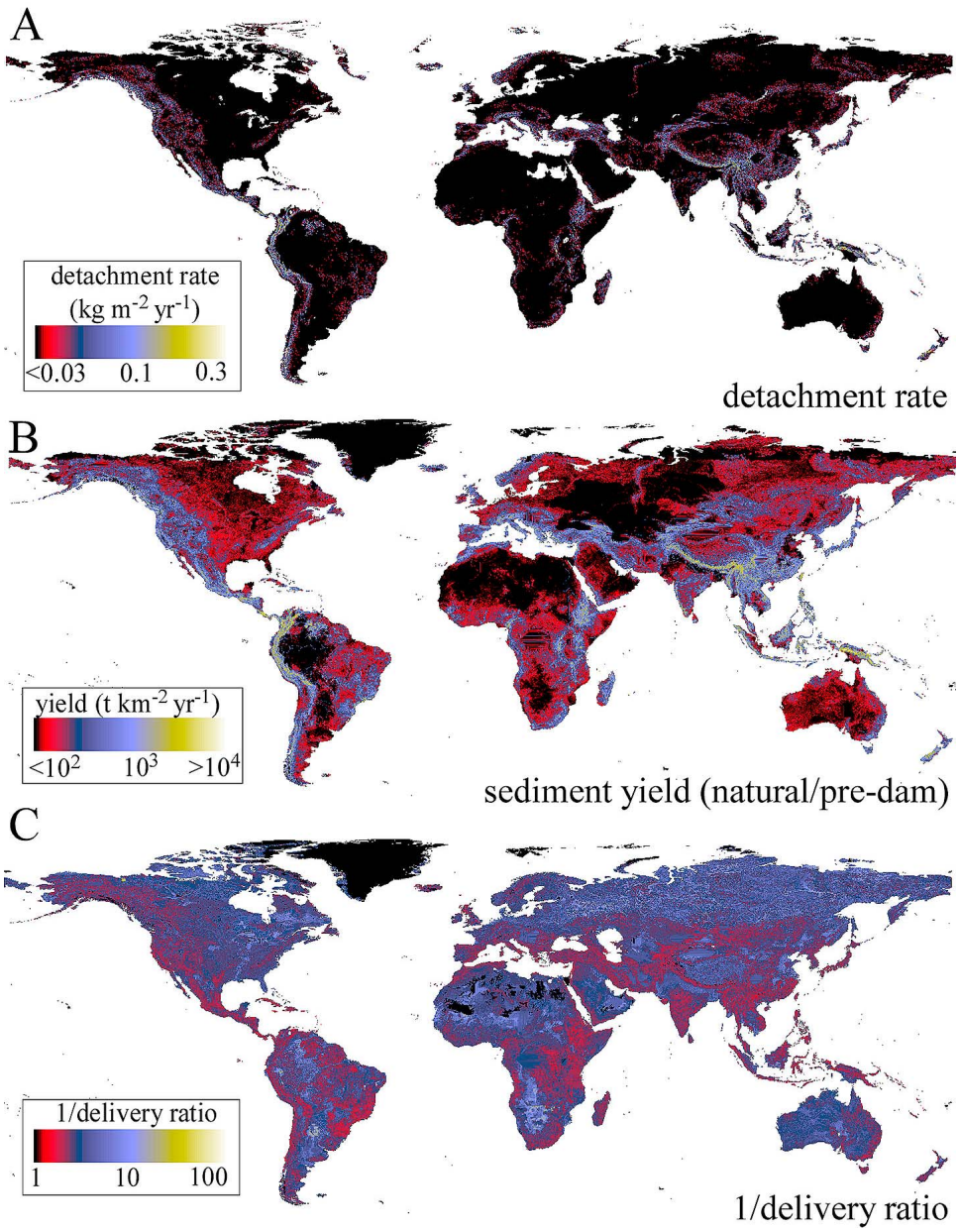

Figure 6. Color maps of the output of the model. (a) Sediment detachment rate, (b) natural/predam suspended sediment yield, and (c) the inverse of the sediment delivery ratio.

Hua Lien and Cho Shui rivers of Taiwan). This interpretation of a sampling bias in the measured data is consistent with the fact that the range of yields predicted by the model matches that of the measured data while the measured data for the smaller basins coincide with the highest yields predicted by the model anywhere in the world.

[32] Figure 8c plots sediment yield as a function of slope for the model predictions and the measured data. The model prediction and measured data are not precisely comparable because the model predictions are plotted against local slope while the measured data are plotted against basin-averaged slope. Despite this difference, both data sets show a similar power law relationship between sediment yield and slope with an exponent of approximately 5/4, reflecting the relationship between detachment rate and slope in (3). The model predicts yields that are somewhat higher than the power law trend for low slopes, however. This deviation is to be expected, however, because many pixels of low slope in the model are relatively large drainage basins where the yield is related not to the local slope but to steeper slopes upstream. The measured data have somewhat higher yields than the average model predictions at a given drainage area (Figure 8b) or slope (Figure 8c). This is likely a consequence of the fact that measured sediment discharges do not represent a random sample but instead are concentrated in more temperate regions on Earth where loads are high compared to the vast but relatively unpopulated/unmeasured arctic regions (which tend to have lower yields for otherwise similar drainage area and slope values based on the temperature dependence of sediment yields).

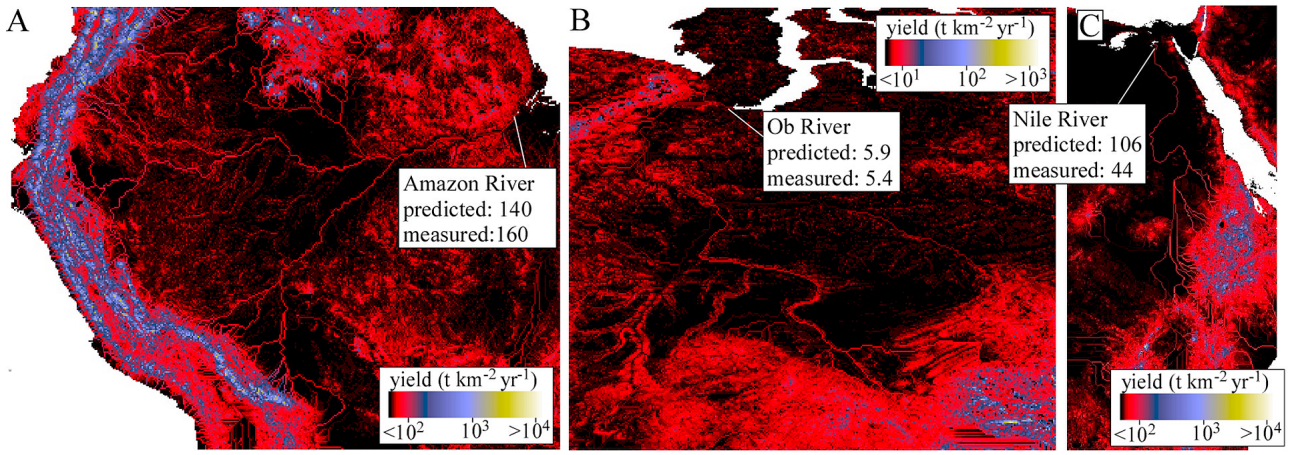

Figure 7. Color maps of the suspended sediment yield predicted by the model for (a) the Amazon basin, (b) the Ob basin, and (c) the Nile basin.

[33] Figure 9 illustrates the sensitivity of the sediment delivery ratios predicted by the model to the exponent assumed in the power function relationship between Rouse number and slope. The results are plotted for exponents of –0.25, –0.5, and –0.75 in Figures 9a–9c, respectively. The results show that as the value of the exponent decreases, i.e., becomes closer to –1, the sediment delivery ratio has a greater dependence on basin area because more of the sediment transported from upstream becomes trapped in lowland channels. Assuming an exponent of –0.25, sediment delivery ratios have no systematic dependence on drainage basin area and continental-scale drainage basins have sediment delivery ratios significantly larger than 0.1. These predictions are inconsistent with observations that show a weak but significant decrease in sediment delivery ratio with increasing basin area. Conversely, assuming an exponent of –1 results in a relatively rapid decrease in sediment delivery ratio with increasing area such that large continental drainage basins transport, on average, only a few percent of the material eroded from upland areas. These results indicate that the model achieves results most consistent with observed data when an exponent of –0.5 is used, as in (6).

4. Discussion

[34] Many researchers have proposed empirical regression models to predict the long-term sediment discharge from drainage basins. It is appropriate to compare the results of this paper with representative examples of those models. *Jansen and Painter* [1974], for example, proposed a regression model with 8 free parameters based on an analysis of 79 large river basins

$$\log q_s = 0.100 \log q_w - 0.314 \log A + 0.750E + 1.104S + 0.368 \log T + 0.786 \log L - 2.324V - 2.032, \quad (7)$$

where q_s is the suspended sediment yield in t km^{-2} yr^{-1} (t is metric tons); q_w is the mean annual runoff in mm; A is the drainage basin area in km^2; E is the mean basin elevation in m; S is the basin relief ratio in m/km; T is the mean basin temperature in °C; L is a lithologic index from 2 (hard rocks) to 6 (soft rocks); and V is an index of vegetation cover from 1 (desert scrub) to 4 (forests). Equation (7) demonstrates that sediment yield increases with increasing runoff, relief, precipitation, temperature, and rock erodibility and decreases with increasing basin area and vegetation cover. One drawback of (7) is the use of qualitative indices for quantifying the effects of lithology/soil texture and vegetation cover. In this paper I improved upon (7) by using quantitative data for soil texture and vegetation cover.

[35] Figure 10a plots the predicted versus observed suspended sediment yields using a three-parameter regression model proposed by *Mulder and Syvitski* [1996, equation 9]

$$\log Q_s = 0.4058 \log A + 1.2789 \log R - 3.679, \quad (8)$$

where Q_s is the suspended sediment discharge in kg s^{-1} and R is the basin relief in m. The data plotted in Figure 10a come from the same long-term suspended sediment discharges of 128 rivers that I used elsewhere in the paper. Equation (8) has been superseded by more recent models of Syvitski and his colleagues that add additional factors for temperature and land use [e.g., *Syvitski et al.*, 2003, 2005; *Syvitski and Milliman*, 2007]. However, it is useful to consider the results of (8) as a baseline against which to compare the results of other proposed models. Equation (8) is limited in two basic ways. First, it tends to overpredict the sediment yield of low-yield rivers and underpredict the yield of high-yield rivers. As Figure 10a illustrates, most of the data points lie above the 1:1 line for low-yield rivers and most of the data points lie below the 1:1 line for high-yield rivers. For example, the yields of the Hua Lien and Cho Shui rivers of Taiwan (the two highest-yield rivers in the database) are underpredicted by approximately a factor of 10, suggesting that (8) is not capturing an important element of the controls on suspended sediment yield in high-yield rivers. Second, (8) produces 3 cases in which the model prediction is more than a factor of 30 higher than the measured data. These are the Oder (Germany), Adour (France), and Tarsus (Turkey) Rivers. *Syvitski et al.* [2003], following *Jansen and Painter* [1974] and *Hovius* [1998], added mean basin temperature to (2) and showed that the resulting model yielded improved

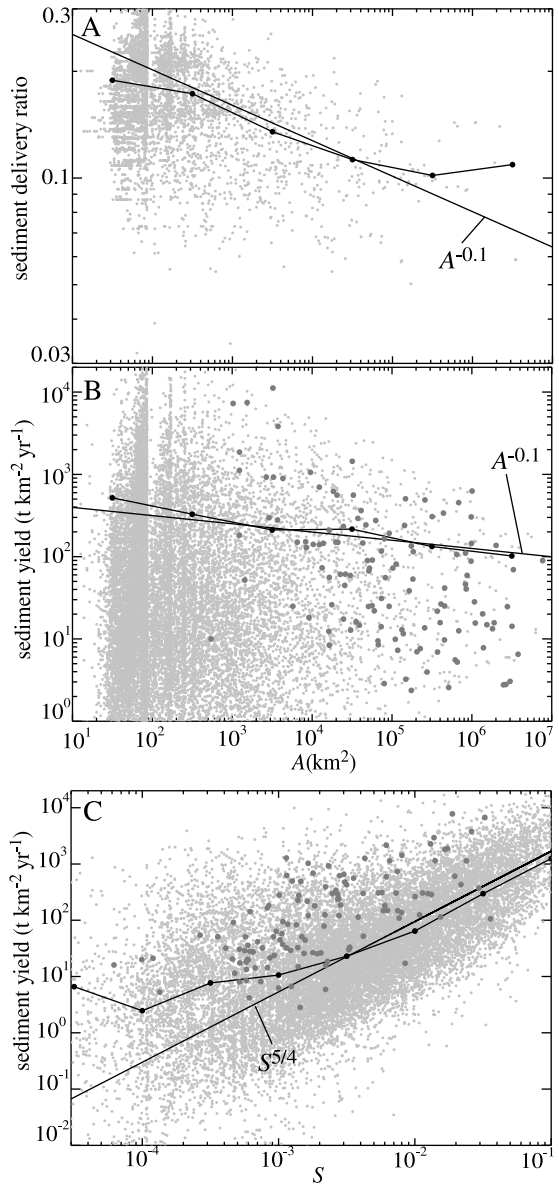

Figure 8. Scaling relationships between suspended sediment yields and delivery ratios predicted by the model. Small, light gray circles are model predictions (a 1% random sample). (a) Plot of the sediment delivery ratio as a function of drainage basin area A and plots of the suspended sediment yield as a function of (b) drainage basin area A and (c) slope S. Larger, darker gray circles in Figures 8b and 8c are measured data for comparison. Black circles joined with lines are averages of the model predictions in logarithmically spaced bins.

results for cold region drainage basins. The resulting ART model of *Syvitski et al.* [2003] is given by

$$Q_s = \alpha_3 A^{\alpha_4} R^{\alpha_5} e^{kT}. \quad (9)$$

One limitation of the ART model is that it does not include precipitation, perhaps the most important climatic variable controlling sediment discharge. Equation (9) also does not include vegetation or lithology/soil texture. *Syvitski et al.* [2003] included precipitation implicitly by calibrating (9) separately to the measured sediment discharges from 5 different zones of latitude and temperature (i.e., larger calibration values of α_3 in the tropics is implicitly a result of higher precipitation in the tropics). Calibrated in this way, the ART model of *Syvitski et al.* [2003] has 20 free parameters.

[36] While the ART model of *Syvitski et al.* [2003] provides a convenient, powerful tool for sediment discharge prediction, it is necessary to weigh model accuracy against model complexity (i.e., the number of free parameters in the model) when evaluating model performance. As the number of free parameters of any model grows, the root-mean-square (RMS) error of that model tends to decrease whether or not the model with more free parameters is actually a better representation of the physical processes at work in the system compared to a model with fewer free parameters.

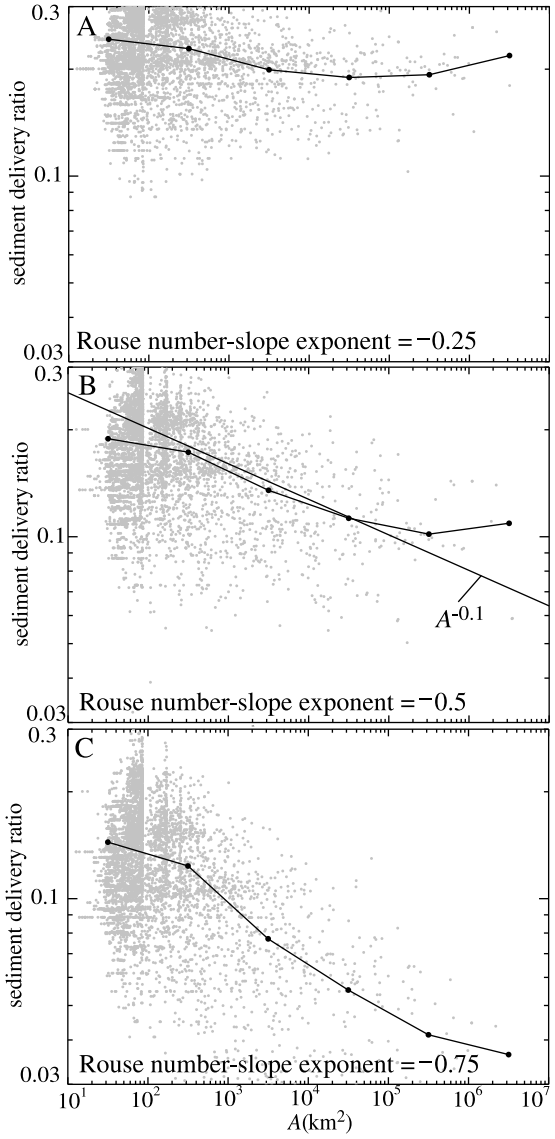

Figure 9. Sensitivity of the model-predicted relationship between sediment delivery ratio and drainage area for three different values of the exponent in the power function relationship between Rouse number and channel slope: (a) −0.25, (b) −0.5, and (c) −0.75.

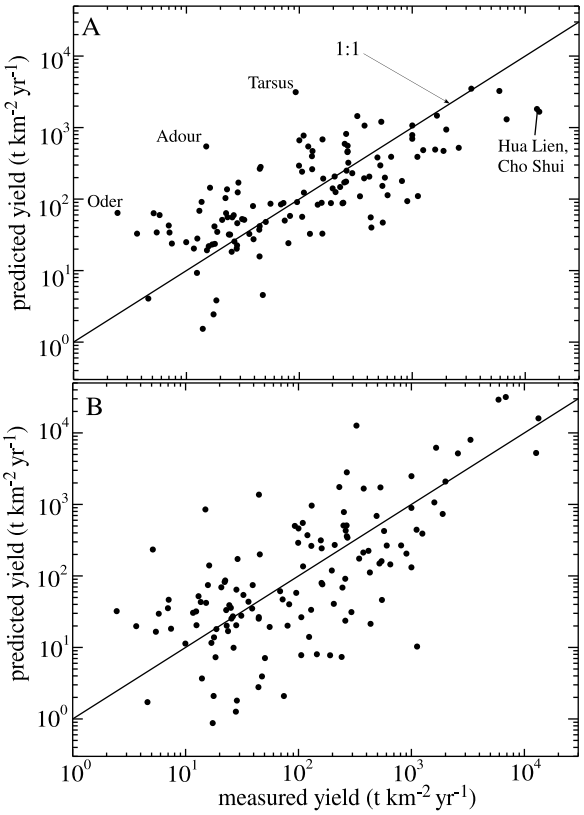

Figure 10. Predicted versus measured suspended sediment yields for (a) equation (9) and (b) equation (11).

In order to choose among competing regression models, therefore, it is not sufficient to simply to choose the model with the highest correlation coefficient or R statistic. Instead, both the mean square error and the number of free parameters must be considered in order to properly assess relative model performance. The standard measure used for this purpose is the Akaike information criterion (*AIC*) [*Akaike*, 1974], defined for cases (as here) without an explicit quantification of measurement error, by the following:

$$AIC = n \ln\left(\frac{RSS}{n}\right) + 2k + \frac{2k(k+1)}{n-k-1}, \tag{10}$$

where *RSS* is the residual sum of squares (equal to the sum of the differences between the logarithms of the predicted and actual data); n is the number of data points; and k is the number of free parameters in the model. The optimum model among a set of competing models is generally the one with the lowest *AIC* value, although other considerations might be relevant, including the realism of the models in relation to the physical processes the model represents and the relative quality of the input data to each model. *AIC* values are useful because they provide an unbiased criterion for evaluating competing models with different numbers of free parameters. The *AIC* value of the model of this paper is –180.7, based on *RSS* and n values of 30.24 and 128, respectively, and the 2 free parameters of the model. Additional free parameters should be added to this or any other regression model only insofar as they lead to improvements that are statistically significant as quantified by a reduction in *AIC*. The *AIC* value of (3) is –149.8 based on an *RSS* value of 37.9 and the 3 free parameters of the model, indicating that (3) is inferior to the model of this paper both on account of its lower accuracy (i.e., *RSS* value) and greater complexity (i.e., k value).

[37] Figure 10b illustrates the results of another standard model against which newer sediment discharge models can be compared. This figure plots the predicted versus measured suspended sediment yields based on the assumption that suspended sediment discharge is proportional to stream power, i.e., the product of mean water discharge and mean basin slope

$$q_s = c\frac{Q}{A}\frac{R}{L_b}, \tag{11}$$

where c is a regression coefficient equal to 5×10^5 when (11) is calibrated to the 128-river database of this paper; Q is the mean water discharge in $m^3\ s^{-1}$; and L_b is basin length in km. Many geomorphic studies assume that basin-averaged erosion rates are controlled by stream power. This assumption is based on the conceptual model that bedrock channel erosion is controlled by stream power and that hillslope erosion adjusts to keep pace with bedrock channel erosion [e.g., *Whipple and Tucker*, 1999]. While the correlation illustrated in Figure 10b is significant, the fit is clearly worse than that of Figure 10a.

[38] The model of this paper predicts observed sediment yields globally using a model that incorporates all of the principal controls on sediment yield documented in the geomorphic literature and that uses only 2 free parameters. The model represents a good tradeoff between model accuracy and complexity. Significant scatter between the predicted values and observed data remain, however. Many sediment yield studies have noted the uncertainties associated with measured sediment discharge data that likely contribute to this scatter. Among them are: uncertainties of measurement location (some measurements are acquired far from the mouth of a river or at variable locations along a river over time), episodicity of sediment discharges (making good estimates of long-term sediment discharges difficult to obtain from short-term data sets) and the difficulty of adjusting measured data for the impact of dams and recent changes in land use.

[39] Of these potential sources of uncertainty, the episodicity of sediment yields, has been emphasized in recent years. Sediment discharges in some rivers (especially small rivers in relatively arid climates) are sufficiently variable that sediment discharges measured over decadal time scales may not be representative of long-term averages [*Inman and Jenkins*, 1999]. Moreover, if most sediment is discharged in small, rare floods, it may be that sediment discharges measured over decadal time scales underestimate true long-term discharges as a general rule. *Kirchner et al.* [2001], for example, documented that sediment yields measured over decadal time scales were more than a factor of ten smaller than sediment yields determined cosmogenically over time scales of 5 to 27 kyr in drainage basins in Idaho that showed no evidence of alluvial storage. It is important to note, however, that time scales of 5 to 27 kyr include major climatic changes, so differences between short-term and long-term sediment yields may, in part, be due to the fact that

paleoclimatic and paleovegetation conditions (including postfire conditions) were more conducive to erosion compared to modern conditions. Also, it is important to note that rates of fluvial sediment discharge often do not match erosion rates at the hillslope scale for the same reasons that the sediment delivery ratio is rarely measured to be 1. Cosmogenically determined erosion rates measure erosion at the hillslope scale, while sediment yields measure the rates of fluvial transport out of the basin. Studies of sediment budgets in relatively small drainage basins [e.g., *Trimble*, 1977; *Phillips*, 1991] have shown that, even in the absence of field evidence for alluvial storage, sediment delivery ratios are still commonly significantly lower than 1 due to colluvial storage on the lower portions of hillslopes and in low-order valleys. Colluvial processes are important additional components of mass transport/storage that are not accounted for in this or any other study of fluvial sediment discharges. It may be appropriate to consider fluvial sediment yields as representative of erosion/denudation rates over time scales scale much longer than the time scales of hillslope adjustment to tectonic and climatic perturbations (i.e., $\sim 10^6$ yr) [*Fernandes and Dietrich*, 1997] because over such long time scales the supply of sediment from the hillslope to the channel must be balanced by the export of sediment from the channel by fluvial processes. Nevertheless, colluvial transport from hillslopes to channels and fluvial export out of the channel can be expected to be out of equilibrium for long periods of geologic time. In summary, attempts to reconcile erosion rates determined by sediment yields with erosion rates determined by cosmogenic or thermochronologic techniques should acknowledge that sediment yields only capture a portion of total erosion at the hillslope scale. This discussion is not meant to imply that episodicity in sediment discharges does not pose a challenge to accurate assessments of long-term sediment discharge estimation. Instead, the point is simply that decadal-scale sediment discharge measurements can, in many cases, provide reasonably accurate estimates for long-term sediment discharges. Moreover, discrepancies between sediment yields and erosion rates determined cosmogenically or thermochronologically do not necessarily imply a failure of sediment yields to measure long-term erosion rates.

[40] One important limitation of the model of this paper is that landsliding is not explicitly included. The model of this paper assumes a weakly nonlinear relationship between detachment from hillslopes and slope. That relationship is motivated from relationships used in RUSLE and the desire for a parsimonious functional form between suspended sediment yield and slope. The resulting model does a good job of reproducing the observed variation between suspended sediment yield and basin slope in the data set of 128 global rivers considered here (Figure 8c), but the model nonetheless systematically underestimates the suspended sediment yields of basins in the data set with the highest values, i.e., greater than 10^3 t/km^2/yr. One approach to including landsliding explicitly in the model of this paper would be to adopt a more nonlinear relationship between sediment flux and slope for steep slopes, e.g., [*Roering et al.*, 1999]

$$S_f = \frac{1}{1 - (S/S_c)^2}, \tag{12}$$

where S_c is a threshold angle of stability. Such an approach, however, would come at the cost of introducing another free parameter in the model and would likely require high-resolution input DEM data (30 m or better) in order to resolve slopes accurately enough for the sensitive dependence between detachment rate and slope in (12).

[41] The model of this paper is based on input data computed at 5 arc min resolution (i.e., approximately 10 km at the equator). In the future, as the model is applied using input data with finer scales of resolution, the calibration parameters will likely need to be adjusted to reflect the fact that extremes of slope and bare vegetation will be greater in higher-resolution input data sets. The finite resolution of the model limits its ability to resolve small areas of steep slopes, bare vegetation, etc. that can have a large influence on suspended sediment yields. Future research will examine the scaling of the model behavior with respect to the resolution of the input data.

[42] *Hovius* [1998] documented the importance of uplift rate in controlling sediment yields globally. Uplift rate correlates with slope, hence the model of this paper is partly consistent with the results of *Hovius* [1998]. In very active mountain belts, however, it is likely that slope/relief reaches a maximum point beyond which an increase in uplift rate causes further increases in sediment yield without a corresponding increase in slope. The model of this paper likely underestimates the sediment yield in such highly active tectonic regions where sediment yield is controlled by rock uplift rate. A more sophisticated model would include rock uplift rates from around the world and, where the predicted sediment discharge is less than the observed discharge, the rock uplift rate would be used as an input to calculating the detachment rate. Available data on rock uplift rates lack sufficient spatial coverage to make this approach feasible at this time, however.

[43] The model of this paper does not consider the effects of dams and/or recent land use changes (including agriculture). *Wilkinson and McElroy* [2007] reviewed available evidence and concluded that the rate of soil loss in croplands is approximately four times the global suspended sediment discharge to the ocean. How much of this eroded soil is transported as suspended load versus bed load and how much of it makes its way into major rivers hundreds to thousands of kilometers downstream from agricultural sources is not well constrained, however. The fact that agricultural erosion on Earth is estimated to be almost four times higher than the sediment flux to the ocean suggests that the vast majority of sediment eroded from crops is stored in dams and/or lowland floodplains. It may be that impoundment of sediment behind dams traps a larger proportion of the total sediment (including sediments from both natural and human-induced erosion) in agricultural areas where the prevalence of dams is also greatest. *Syvitski and Milliman* [2007] attempted to quantify the influence of humans on suspended sediment loads by adding additional parameters to the ART and QRT models, including those designed to capture the effects of sediment trapping and human-induced erosion. As these authors note, however, these effects are difficult to quantify with confidence. For example, *Syvitski and Milliman* [2007] concluded that the Mississippi River basin had either a sufficiently low human footprint (or a mix of mutually negating factors) (see their Figure 7) that no adjustment of model prediction for

human-induced erosion was deemed necessary in that basin. This is difficult to reconcile with the results of *Wilkinson and McElroy* [2007], who showed that the vast majority of the area of the Mississippi River basin has cropland sediment yields that are 1–2 orders of magnitude larger than natural erosion rates (see their Figures 6 and 8). These results point to the need for more research to quantify the effects of agricultural soil erosion on sediment yields of large drainage basins.

5. Conclusions

[44] The suspended sediment yield of a drainage basin is controlled by slope, precipitation, temperature, vegetation, soil texture and their spatial variations in that drainage basin. In this paper I took a spatially distributed approach to quantifying these controls on suspended sediment yields for drainage basins globally. The spatially distributed nature of the model and in its inclusion of vegetation cover (quantified as LAI) and soil texture model make it novel among existing models for predicting global sediment discharges/yields. The resulting model maximizes the accuracy of the model prediction for a minimum number of free parameters. The model explicitly distinguishes the detachment of sediment on hillslopes from the transport of sediment in channels. The model uses slope, soil texture, and mean monthly rainfall and leaf area index as controlling parameters for the detachment component. The transport component is modeled using a Rouse number–dependent transport criterion that explicitly includes the effects of slope and soil texture. The transport component of the model allows for size selective sediment transport or storage with the result that the model simultaneously reproduced both the long-term sediment yield of 128 global rivers with a Pearson correlation coefficient (R^2 value) of 0.79 and sediment delivery ratios that are consistent with those measured in natural drainage basins. The model can serve as a baseline for studies aimed at understanding the sensitivity of suspended sediment yields to changes in climate and tectonics over a range of time scales.

[45] **Acknowledgments.** This study was made possible by a grant from ExxonMobil Corporation. I wish to thank Mike Blum for helpful conversations prior to submission and Liz Safran, Brandon McElroy, Rob Ferguson, Associate Editor John Pitlick, and Editor Alex Densmore for helpful reviews/comments during the review process that greatly improved the paper.

References

Ahnert, F. (1970), Functional relationships between denudation, relief, and uplift in large, mid-latitude drainage basins, *Am. J. Sci.*, *268*, 243–263, doi:10.2475/ajs.268.3.243.

Akaike, H. (1974), A new look at the statistical model identification, *IEEE Trans. Autom. Control*, *19*(6), 716–723, doi:10.1109/TAC.1974.1100705.

Beusen, A. H. W., A. L. M. Dekkers, A. F. Bouwman, W. Ludwig, and J. Harrison (2005), Estimation of global river transport of sediments and associated particulate C, N, and P, *Global Biogeochem. Cycles*, *19*, GB4S05, doi:10.1029/2005GB002453.

de Vente, J., J. Poesen, M. Arabkhedri, and G. Verstraeten (2007), The sediment delivery problem revisited, *Prog. Phys. Geogr.*, *31*, 155–178, doi:10.1177/0309133307076485.

Douglas, I. (1967), Man, vegetation and the sediment yield of rivers, *Nature*, *215*, 925–928, doi:10.1038/215925a0.

Dunne, T. (1979), Sediment yield and land use in tropical catchments, *J. Hydrol.*, *42*, 281–300, doi:10.1016/0022-1694(79)90052-0.

Ferguson, R. I., and M. Church (2004), A simple universal equation for grain settling velocity, *J. Sediment. Res.*, *74*, 933–937, doi:10.1306/051204740933.

Fernandes, N. F., and W. E. Dietrich (1997), Hillslope evolution by diffusive processes: The timescale for equilibrium adjustments, *Water Resour. Res.*, *33*(6), 1307–1318, doi:10.1029/97WR00534.

Fournier, F. (1960), *Climat et Érosion*, 201 pp., Presses Univ. de Fr., Paris.

Hay, W. W., M. J. Rosol, J. L. Sloan II, and D. E. Jory (1988), Plate tectonic control of global patterns of detrital and carbonate sedimentation, in *Carbonate-Clastic Transitions*, *Dev. Sedimentol.*, vol. 42, edited by L. J. Doyle and H. H. Roberts, pp. 1–34, Elsevier, Amsterdam, doi:10.1016/S0070-4571(08)70163-8.

Hijmans, R. J., S. E. Cameron, J. L. Parra, P. G. Jones, and A. Jarvis (2005), Very high resolution interpolated climate surfaces for global land areas, *Int. J. Climatol.*, *25*, 1965–1978, doi:10.1002/joc.1276.

Hooke, R. L. (2000), On the history of humans as geomorphic agents, *Geology*, *28*, 843–846, doi:10.1130/0091-7613(2000)28<843:OTHOHA>2.0.CO;2.

Hovius, N. (1998), Controls on sediment supply by large rivers, in *Relative Role of Eustasy, Climate, and Tectonism in Continental Rocks*, edited by K. W. Shanley and P. J. McCabe, *Spec. Publ. SEPM Soc. Sediment. Geol.*, *59*, 2–16, doi:10.2110/pec.98.59.0002.

Inman, D. L., and S. A. Jenkins (1999), Climate change and the episodicity of sediment flux of small California rivers, *J. Geol.*, *107*, 251–270, doi:10.1086/314346.

Jansen, I. M. L., and R. B. Painter (1974), Predicting sediment yield from climate and topography, *J. Hydrol.*, *21*, 371–380, doi:10.1016/S0022-1694(74)80006-5.

Kirchner, J. W., R. C. Finkel, C. S. Riebe, D. E. Granger, J. L. Clayton, J. G. King, and W. F. Megahan (2001), Mountain erosion over 10 yr, 10 k.y., and 10 m.y. time scales, *Geology*, *29*, 591–594, doi:10.1130/0091-7613(2001)029<0591:MEOYKY>2.0.CO;2.

Laflen, J. M., L. J. Lane, and G. R. Foster (1991), WEPP: A next generation of erosion prediction technology, *J. Soil Water Conserv.*, *46*(1), 34–38.

Langbein, W. B., and S. A. Schumm (1958), Yield of sediment in relation to mean annual precipitation, *Eos Trans. AGU*, *39*, 1076.

Ludwig, W., and J.-L. Probst (1998), River sediment discharge to the oceans; present-day controls and global budgets, *Am. J. Sci.*, *298*, 265–295, doi:10.2475/ajs.298.4.265.

McCool, D. K., L. C. Brown, G. R. Foster, C. K. Mutchler, and L. D. Meyer (1987), Revised slope steepness factor for the universal soil loss equation, *Trans. ASAE*, *30*, 1387–1396.

Meade, R. H. (1982), Sources, sinks, and storage of river sediment in the Atlantic drainage of the United States, *J. Geol.*, *90*, 235–252, doi:10.1086/628677.

Milliman, J. D., and J. P. M. Syvitski (1992), Geomorphic/tectonic control of sediment discharge to the ocean: The importance of small mountainous rivers, *J. Geol.*, *100*, 525–544, doi:10.1086/629606.

Milliman, J. D., Y.-S. Qin, M.-E. Ren, and Y. Saito (1987), Man's influence on the erosion and transport of sediment by Asian rivers: The Yellow River (Huanghe) example, *J. Geol.*, *95*, 751–762, doi:10.1086/629175.

Montgomery, D. R., and M. T. Brandon (2002), Topographic controls on erosion rates in tectonically active mountain ranges, *Earth Planet. Sci. Lett.*, *201*, 481–489, doi:10.1016/S0012-821X(02)00725-2.

Mulder, T., and J. P. M. Syvitski (1995), Turbidity currents generated at river mouths during exceptional discharges to the world oceans, *J. Geol.*, *103*, 285–299, doi:10.1086/629747.

Mulder, T., and J. P. M. Syvitski (1996), Climatic and morphologic relationships of rivers: Implications of sea-level fluctuations on river loads, *J. Geol.*, *104*, 509–523, doi:10.1086/629849.

Nearing, M. A. (1997), A single, continuous function for slope steepness influence on soil loss, *Soil Sci. Soc. Am. J.*, *61*, 917–919, doi:10.2136/sssaj1997.03615995006100030029x.

Ohmori, H. (1983), Erosion rates and their relation to vegetation from the viewpoint of world-wide distribution, *Bull. Dep. Geogr. Univ. Tokyo*, *15*, 77–91.

Osterkamp, W. R., and T. J. Toy (1997), Geomorphic considerations for erosion prediction, *Environ. Geol.*, *29*, 152–157, doi:10.1007/s002540050113.

Paola, C. (2000), Quantitative models of sedimentary basin filling, *Sedimentology*, *47*, 121–178, doi:10.1046/j.1365-3091.2000.00006.x.

Peucker-Ehrenbrink, B. (2009), Land2Sea database of river drainage basin sizes, annual water discharges, and suspended sediment discharge, *Geochem. Geophys. Geosyst.*, *10*, Q06014, doi:10.1029/2008GC002356.

Phillips, J. D. (1991), Fluvial sediment budgets in the North Carolina Piedmont, *Geomorphology*, *4*, 231–241, doi:10.1016/0169-555X(91)90006-V.

Pinet, P., and M. Souriau (1988), Continental erosion and large-scale relief, *Tectonics*, *7*, 563–582, doi:10.1029/TC007i003p00563.

Prosser, I. P., and W. E. Dietrich (1995), Field experiments on erosion by overland flow and their implication for a digital terrain model of channel

initiation, *Water Resour. Res.*, *31*(11), 2867–2876, doi:10.1029/95WR02218.

Restrepo, J. D., B. Kjerfve, M. Hermelin, and J. C. Restrepo (2006), Factors controlling sediment yield in a major South American drainage basin: The Magdalena River, Colombia, *J. Hydrol.*, *316*, 213–232, doi:10.1016/j.jhydrol.2005.05.002.

Roehl, J. W. (1962), Sediment source areas, delivery ratios, and influencing morphological factors, *Inter. Assoc. Sci. Hydrol. Publ.*, *59*, 202–213.

Roering, J. J., J. W. Kirchner, and W. E. Dietrich (1999), Evidence for nonlinear, diffusive sediment transport on hillslopes and implications for landscape morphology, *Water Resour. Res.*, *35*(3), 853–870, doi:10.1029/1998WR900090.

Schumm, S. A. (1963), The disparity between present rates of denudation and orogeny, *U.S. Geol. Surv. Prof. Pap.*, *454-H*, 13 pp.

Sellers, P. J., C. J. Tucker, G. J. Collatz, S. O. Los, C. O. Justice, D. A. Dazlich, and D. A. Randall (1996), A revised land surface parameterization (SiB2) for atmospheric GCMS. Part II: The generation of global fields of terrestrial biophysical parameters from satellite data, *J. Clim.*, *9*, 706–737, doi:10.1175/1520-0442(1996)009<0706:ARLSPF>2.0.CO;2.

Summerfield, M. A., and N. J. Hulton (1994), Natural controls of fluvial denudation rates in major world drainage basins, *J. Geophys. Res.*, *99*, 13,871–13,883, doi:10.1029/94JB00715.

Syvitski, J. P. M., and J. D. Milliman (2007), Geology, geography, and humans battle for dominance over the delivery of fluvial sediment to the coastal ocean, *J. Geol.*, *115*, 1–19, doi:10.1086/509246.

Syvitski, J. P. M., S. D. Peckham, R. Hilberman, and T. Mulder (2003), Predicting the terrestrial flux of sediment to the global ocean: A planetary perspective, *Sediment. Geol.*, *162*, 5–24, doi:10.1016/S0037-0738(03)00232-X.

Syvitski, J. P. M., C. J. Vörösmarty, A. J. Kettner, and P. Green (2005), Impact of humans on the flux of terrestrial sediment to the global coastal ocean, *Science*, *308*, 376–380, doi:10.1126/science.1109454.

Trimble, S. W. (1977), The fallacy of stream equilibrium in contemporary denudation studies, *Am. J. Sci.*, *277*, 876–887, doi:10.2475/ajs.277.7.876.

Tucker, C. J., J. E. Pinzon, and M. E. Brown (2004), Global Inventory Modeling and Mapping Studies, version 2.0, http://glcf.umiacs.umd.edu/data/gimms/, Global Land Cover Facil., Univ. of Md., College Park.

Turowski, J. M., D. Rickenmann, and S. J. Dadson (2010), The partitioning of the total sediment load of a river into suspended load and bedload: A review of empirical data, *Sedimentology*, *57*, 1126–1146, doi:10.1111/j.1365-3091.2009.01140.x.

Vanacker, V., F. von Blanckenburg, G. Govers, A. Molina, J. Poesen, J. Deckers, and P. Kubik (2007), Restoring dense vegetation can slow mountain erosion to near benchmark levels, *Geology*, *35*, 303–306, doi:10.1130/G23109A.1.

Walling, D. E. (1983), The sediment delivery problem, *J. Hydrol.*, *65*, 209–237, doi:10.1016/0022-1694(83)90217-2.

Whipple, K. X., and G. E. Tucker (1999), Dynamics of the stream-power river incision model: Implications for height limits of mountain ranges, landscape response timescales, and research needs, *J. Geophys. Res.*, *104*(B8), 17,661–17,674, doi:10.1029/1999JB900120.

Wilkinson, B. H., and B. J. McElroy (2007), The impact of humans on continental erosion and sedimentation, *Geol. Soc. Am. Bull.*, *119*, 140–156, doi:10.1130/B25899.1.

Wilson, L. (1973), Variations in mean annual sediment yield as a function of mean annual precipitation, *Am. J. Sci.*, *273*, 335–349, doi:10.2475/ajs.273.4.335.

Wischmeier, W. H., and D. D. Smith (1978), Predicting rainfall erosion losses: A guide to conservation planning, *Agric. Handb. 537*, U.S. Dep. of Agric., Washington, D. C.

Young, A. (1969), Present rate of land erosion, *Nature*, *224*, 851–852, doi:10.1038/224851a0.